

RSC Advances



This is an *Accepted Manuscript*, which has been through the Royal Society of Chemistry peer review process and has been accepted for publication.

Accepted Manuscripts are published online shortly after acceptance, before technical editing, formatting and proof reading. Using this free service, authors can make their results available to the community, in citable form, before we publish the edited article. This *Accepted Manuscript* will be replaced by the edited, formatted and paginated article as soon as this is available.

You can find more information about *Accepted Manuscripts* in the [Information for Authors](#).

Please note that technical editing may introduce minor changes to the text and/or graphics, which may alter content. The journal's standard [Terms & Conditions](#) and the [Ethical guidelines](#) still apply. In no event shall the Royal Society of Chemistry be held responsible for any errors or omissions in this *Accepted Manuscript* or any consequences arising from the use of any information it contains.



Supercritical CO₂ synthesized TiO₂ nanowires covalently linked with core-shell CdS-ZnS quantum dots: Enhanced photocatalysis and stability

Md Abdul Mumin, Golam Moula and Paul A. Charpentier*

Semiconductor quantum dots (QDs) sensitized onto nano TiO₂ as heterogeneous photocatalysts have drawn considerable interest over the past few years. However, stability of the QDs attached to TiO₂ and consistent photocatalysis are still a major challenges of this approach. We describe herein, a facile process to fabricate nanocomposites from porous TiO₂ nanowires and bare CdS and core-shell CdS-ZnS QDs, where the QD particles are linked covalently to the titania surface through a bifunctional organic linker, mercapto propionic acid (MPA). A thin layer of ZnS was grown on 6 nm CdS QDs to restrain the photocorrosion and passivate the trap states, enhancing the photoluminescence and quantum yield. The bifunctional linking molecule, MPA, was found to effectively disperse and stabilize the QD nanoparticles. The photocatalytic activities of the prepared catalysts were evaluated under ultraviolet and visible light solar irradiation for the photodegradation of methylene blue (MB), an organic dye. The decomposition rate of MB was enhanced as follows: CdS-ZnS-MPA-TiO₂ > CdS-MPA-TiO₂ > CdS-ZnS-TiO₂ > CdS-TiO₂ > TiO₂ > P25. A maximum photodegradation efficiency of MB dye (~88%) was obtained by core-shell CdS-ZnS QDs linked with nanoTiO₂. After 3 cycling tests of degradation, the loss of photoactivity was significantly minimized (from 68% to 10%) by CdS-ZnS-MPA-TiO₂ compared to CdS-ZnS-TiO₂ (by direct deposition).

Received 00th January 20xx,
Accepted 00th January 20xx

DOI: 10.1039/x0xx00000x

www.rsc.org/

1. Introduction

Nanosized Titanium dioxide (TiO₂), one of the most promising photocatalysts, has been extensively investigated for several decades in the area of solar cells and photocatalysis [1-3]. TiO₂ has several advantages owing to its low cost, abundance, nontoxicity, good stability, and unique optoelectronic properties [4]. However, due to its wide band gap (3.2 eV), TiO₂ can only be excited by a small UV fraction (less than 6 %) of solar light, making it impractical for use under natural sunlight [5]. The photogenerated electrons/holes are easily consumed via recombination, resulting in a low quantum yield and poor efficiency in these applications [6].

To break the bottleneck, there have been various attempts to enhance and expand the optical absorption range of TiO₂ and improve the separation efficiency of photogenerated electron-hole pairs. Recently, semiconductor quantum dots (QDs) have been attracting extensive attention to sensitize TiO₂ due to their unique size dependent optoelectronic properties and the possibility of multiexciton generation. A lower band gap QD like CdSe, CdS with higher conduction band (CB) can enhance the electronic conversion efficiency of TiO₂ [7-9]. The photogenerated electrons from the CB of the light activated QD can be injected into the non-activated

TiO₂, while the holes remain on the QD particles, leading to efficient and longer charge separation, increased UV absorption, as well as extending the absorption to the visible range [10-11]. But, uniform deposition and stability of QD particles on TiO₂ is often a problem due to the lack of attachment approaches and poor surface interactions under typical experimental conditions [12]. A favourable link between QDs and TiO₂ nanoparticles can minimize these drawbacks, also enhancing the transfer of electron injection [7,13].

Recently, intensive efforts have been undertaken to link bare QDs with nano TiO₂ for photocatalysis applications [14-16]. Mostly, long aging time (more than 24 hours) and high temperatures (200 - 400 °C) are required for improving the coupling of the two semiconductor materials and their crystallinity [17]. In previous works, most attention has been paid to the synthesis and optical properties rather than activity and stability during photodegradation. Possible interactions between porous 1D TiO₂ nanostructures and the effect of the bifunctional linking molecules to core-shell QDs needs to be investigated. Although, it has been reported by many researchers that compared to bare QDs, core-shell structured QDs with a thin shell of a higher band gap element are advantageous and have been shown to enhance photo-physical properties [18-20]. This is attributed to the surface defects in the core acting as temporary 'traps' for the electron, hole or excitons, quenching radiative recombination and reducing the quantum yield (QY) [21]. Notably, CdS is an important photosensitizer of TiO₂ and its size dependent optical properties have also been observed and reported by many researchers [6,22]. Recently, we have shown

Department of Chemical and Biochemical Engineering, University of Western Ontario, London Ontario, Canada N6A 5B9

* pcharpentier@eng.uwo.ca; Tel: (519) 661-3466; Fax: (519) 661-3498

that, by forming a thin shell of ZnS on CdS cores, the QY can be improved up to 50%, which is usually less than 20% for bare CdS QDs [23]. The thin shell also minimizes the surface crystal defects and aggregation tendency of CdS, resulting in better particle separation which is very important for the photosensitization of TiO₂ catalyst. Therefore, it is anticipated that by developing a novel facile coupling approach for more quantum efficient and stable core-shell QDs with nanoTiO₂ using mild conditions, the activity and stability of the TiO₂ photocatalyst can be improved.

Supercritical CO₂ (scCO₂) has emerged as a viable "green" alternative to hazardous organic solvents, as CO₂ is cheap, non-toxic, non-flammable, and environmentally benign with low critical temperature and pressure ($T_c = 31.1\text{ }^\circ\text{C}$, $P_c = 7.38\text{ MPa}$). [24]. The unique advantages of scCO₂ include: (i) a "zero" surface tension, allowing penetration into pores that is not possible with organic solvents, (ii) low gas-like viscosities that enhance mass transfer and reaction kinetics, (iii) a liquid-like density and a gas-like diffusivity, and the solubility of solute is tuneable with both temperature and pressure [25]. We recently reported that TiO₂ nanowires synthesized using a sol-gel method in supercritical carbon dioxide (scCO₂) are nano-structured with high specific surface area and porosity, and anatase in nature [25-28]. During sol-gel chemistry, scCO₂ has several roles, acting as a solvent, a modification agent, and a cleaning and a drying agent. [29].

Structurally, TiO₂ exists in three polymorphs: anatase, rutile, and brookite. It is well accepted that anatase TiO₂ exhibits higher photocatalytic activities than rutile and brookite TiO₂ [30,31]. The indirect band gap anatase shows a longer charge carrier lifetime to participate in surface reactions compared to direct band gap rutile and brookite TiO₂. Anatase TiO₂ also enhances faster migration of photogenerated electrons and holes from the interior to the surface, resulting in a lower recombination rate for charge carriers [30,31]. However, the anatase phase is thermodynamically metastable, so synthesis of anatase TiO₂ with better quality including thermal stability is always an important parameter [13]. Compared to TiO₂ nanoparticles, TiO₂ nanowires or nanotubes have been shown to be more effective in solar harvesting applications as their orientation provides excellent percolation pathways for vectorial charge transfer [7]. Thakur et al. [1-] observed that the presence of CdS hinders the transformation of anatase to rutile even after annealing at 600 °C, attributed to the surface defect sites of anatase particles being occupied by CdS [10]. However, they observed no specific morphology of both CdS and TiO₂ nanoparticles and irregular distribution. Therefore, besides the one-dimensional orientation and well crystallized anatase, the strong interactions and uniform distribution of quantum efficient QDs (e.g. core-shell QDs) with TiO₂ is still a major challenge that plays a key role to enhance both the activity and stability of the nanocomposite catalysts.

In the present work, highly photoluminescent and monodispersed CdS bare and CdS-ZnS core-shell quantum dots were prepared by using a facile and modified (changing reaction temperature and duration) colloidal synthesis approach. TiO₂ nanowires were synthesized in scCO₂ using sol-gel polycondensation of Ti-alkoxides and acetic acid. Then, by using a novel facile approach, calcined TiO₂ nanowires were functionalized by a commercially available bifunctional linker (mercapto-propionic acid) and covalently attached to bare or core-shell QDs. The photocatalyst samples were characterized in detail and the energy transfer mechanism

investigated. Finally, the experimental catalysts were investigated for degradation of methylene blue, an organic dye under UV, visible, and also simulated solar lights and the results compared with bare TiO₂ and directly deposited QDs in TiO₂.

2. Experimental

2.1. Materials

All the reagents were used without further purification unless stated otherwise. Instrumental grade CO₂ (99.5% purity) was purchased from Praxair. Argon (ultra high purity, 99.9%, PRAXAIR). Titanium isopropoxide (TIP) (97%), glacial acetic acid (99.99%), Cadmium chloride, sodium diethyldithiocarbamate trihydrate, zinc diethyldithiocarbamate (98%), 3-mercaptopropionic acid (>99%), trioctylamine (TOA) (98%), trioctylphosphine (TOP) (97%), methylene blue (0.05 weight % in water), anhydrous ethanol (≥ 99.5%), methanol (≥ 99.9%), and toluene (≥ 99%) were purchased from Sigma-Aldrich, Canada.

2.2. Synthesis of TiO₂ nanowires

TiO₂ nanowires were synthesized in supercritical carbon dioxide (scCO₂) using a sol-gel technique we reported previously [27]. In a typical experiment, 3 mL of TIP and 9 ml of acetic acid were quickly placed in a 25 mL view cell. The cell was closed and CO₂ was pumped into the view cell using a syringe pump (Isco 260D). Final temperature and pressure were maintained at 60 °C and 6000 psig respectively. Stirring was stopped after 24 h while allowed for five days of aging for complete reaction. After aging, the formed gel was washed using CO₂ at a rate at 0.2 mL/min for 24 h followed by controlled venting at 0.5 mL/min to prevent collapse of the solid network. The resulting powder was then calcined at 450 °C in air (tubular furnace) using a heating rate of 10 °C/min for 2 h.

2.3. Synthesis of CdS and CdS-ZnS QDs

Both bare (CdS) and core-shell (CdS-ZnS) QDs were prepared by following a single-molecular precursor method reported previously [32,33]. To formulate the cadmium precursor, Cd[S₂CN(C₂H₅)₂]₂ for QD synthesis, equimolar (0.1 M) aqueous solutions of sodium diethyldithiocarbamate and cadmium chloride were mixed under vigorous stirring. The rapid reaction yielded a white precipitate that was collected using vacuum filtration. Further purification was achieved by washing with distilled water, and then dried in a vacuum oven overnight at 50 °C. For QD synthesis, in a 250 mL three-necked flask under argon, when the temperature of 50 mL of trioctylamine (TOA) was stable at 235 °C, a solution of 1 g of Cd[S₂CN(C₂H₅)₂]₂ in 18 mL of trioctylphosphine (TOP) was rapidly injected into the flask and continued heating for 20 minutes. During cooling at approximately 75 °C, a large excess of methanol was added followed by separation of the quantum dots through centrifugation. The nanoparticles were then dispersed into toluene and washed with methanol following by centrifugation for at least 3 times. In the case of core-shell (CdS-ZnS) QDs, the temperature of TOA was maintained at 220 °C for 10 minutes after addition of the cadmium diethyldithiocarbamate solution, then a solution of 0.4 g of Zn[S₂CN(C₂H₅)₂]₂ in 6 mL of TOP was slowly added dropwise. After 20 minutes the reaction mixture was cooled and the product separated and washed by following the same method described for the CdS QDs.

2.4. Bifunctional linker coupling

The covalent attachment of CdS and CdS-ZnS QDs to the surface of the TiO₂ nanowires was achieved by using 3-mercaptopropionic acid (MPA), a bifunctional linker. In a 100 mL round bottom flask, 0.25 g of TiO₂ nanowires were introduced in 50 mL of ethanol. After adjusting the pH to 10 by using 0.2M NaOH, 200 μ L of MPA was added to the solution and allowed to react for 4 h. The thiolated TiO₂ nanowires, in which strong Ti-O-C bonds are formed as a result of the reaction of the hydroxy groups of the titania surface with the carboxylic acid groups of MPA, were collected as a precipitate. In a subsequent reaction, the functionalized TiO₂ nanowires were dispersed in 60 mL of THF. After adding QD nanoparticles (2, 5, 10, and 20 wt% with respect to TiO₂), the reaction was kept under argon atmosphere at 55°C for 4 h. The resulting composite particles were collected by washing with ethanol and dried in a vacuum oven overnight.

Direct deposition of QDs on TiO₂ was carried out following the previously reported method [7].

2.5. Material characterization

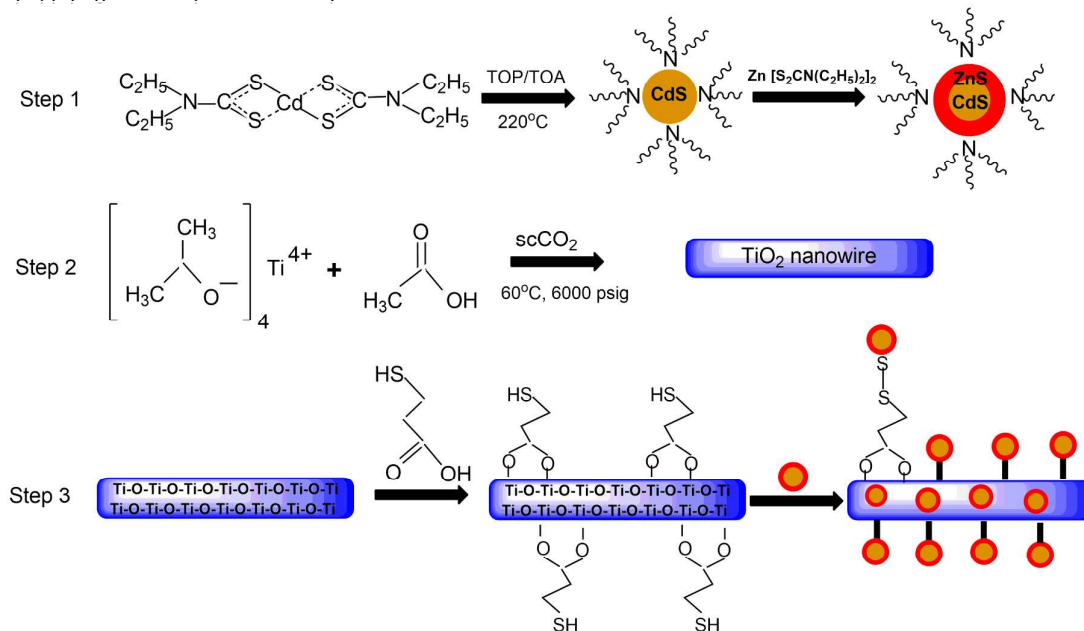
X-ray diffraction (XRD) with a Bruker D2 Phaser bench-top X-ray powder diffractometer using Cu K α radiation (λ for K α =1.54059 Å) at 30 kV and 10 mA was used to investigate the crystalline structure and chemical composition. Dry powder samples were used with patterns collected in step-scan mode with a small grazing angle of incident X-ray with a 2 θ scan range of 10-80 and a step size of 0.25. Transmission electron microscopy (TEM) images were recorded on a Philips CM10 TEM to image the samples to observe their size and shape at 80 kV. The TEM samples were prepared by drop casting ethanol dispersed samples on a copper grid covered with carbon film. Scanning electron microscopy (SEM) was also done by using a LEO(ZEISS) 1540XB FIB/SEM. Samples for SEM imaging were prepared by applying the nanopowder directly to aluminium stubs

on carbon adhesion tape. Elemental composition was confirmed and quantified using the energy dispersive X-ray detection (EDX) feature of the SEM. A Shimadzu UV-3600 UV-VIS-NIR spectrophotometer was used to measure the absorption spectrum of the photocatalyst samples and also methylene blue during photocatalytic activity studies. Infrared spectra were collected from 500 to 4000 cm⁻¹ using a Nicolet 6700 FTIR spectrometer. The XPS analyses were carried out with a Kratos Axis Ultra spectrometer using a monochromatic Al K α source (15mA, 14kV).

2.6. Photocatalytic activity measurements

Photodegradation of Methylene blue (MB), an organic dye was evaluated for both QDs-linker-TiO₂ and QDs-TiO₂ samples, under UV and solar irradiation. All experiments were conducted at room temperature in air. Typically, 0.08 g of as-synthesized catalyst was dispersed in 60 mL of MB solution (10 mg/L in water). For UV illumination, a 125 W high pressure mercury lamp (UVP-Blak-Ray, Model B 100AP) was used that emits UV light (365 and 313 nm). A solar simulator (Model: 69907 Newport) with a 100 W xenon lamp equipped with an air mass filter and a UV cut-off filter (< 365 nm) provided the visible light source.

Prior to irradiation, the Pyrex beaker containing the dispersion was stored in the dark for 30 min to reach adsorption/desorption equilibrium. At a given time interval, 4 mL aliquots were sampled and centrifuged (6000 rpm, 10 min) to separate the particles. The MB concentration in the aliquots was measured by UV-visible spectrophotometer monitoring the absorption maximum at 664 nm. A calibration plot was established relating the absorbance to the concentrations of MB. In each case, blank experiments were also conducted with the catalysts in the absence of light and MB without the catalysts under light irradiation. Moreover, reference experiments were also performed under the same conditions with commercial TiO₂ (Degussa, P25) and synthesized TiO₂ nanowires.



Scheme 1. Schematic illustration of (step 1) chemical reactions of bare CdS and core-shell CdS-ZnS QDs from single molecule precursors, (step 2) TiO₂ nanowires formation in scCO₂ using sol-gel method, and (step 3) functionalization of TiO₂ nanowires and covalent linking with QDs.

The photodegradation of MB for CdSZnS-MPA-TiO₂ nanowires was also carried out under simulated sunlight (Model:LZCX1CH1, Luzchem, Canada, 300W Xenon Lamp) without using any UV cut off filter for two intensities, 14 and 28 mW/cm² and variable catalyst loading concentrations. The UV intensity was measured by using a UV A/B meter (Model: ST513, Sper Scientific Ltd). To examine the production of hydroxyl radical (OH•) during photocatalytic reaction, a 3x10⁻⁴ M terephthalic acid solution in dilute NaOH solution (2x10⁻³ M) was mixed with the experimental photocatalysts under UV light illumination (intensity = 11.05 mW/cm²) [34]. Then the photoluminescence (PL) emission at 425 nm was observed at different intervals using the excitation wavelength of 315 nm [35].

3. Results and discussions

3.1 Morphology and structural characteristics

The crystallization or polymorphs of the TiO₂ framework is a key factor for any application that utilizes its semiconductor properties [14]. Crystalline structure and approximate particle size of both types of QDs were determined using XRD analysis. Figure 1 presents the XRD patterns of both the bare and core-shell QDs, TiO₂ nanowires, and TiO₂ nanocomposites covalently linked with both the bare and core-shell QDs. The bare CdS QDs show the most intense peaks at 2θ values of 24.2, 25.9, 27.8, 36.2, 43.5, 48, and 51.8, matched perfectly with the (100), (002), (101), (102), (110), (103), and (112) of wurtzite (hexagonal) phase of CdS (ICDD PDF 02-1310) [19].

Splitting to three peaks at angles (2θ degree) 24-30 region represents the formation of hexagonal crystallinity rather than a single broad peak representing the cubic CdS QDs [36]. In the case of CdS-ZnS core-shell QDs, the slight increase of the peaks at 28.2, 43.9, and 52.1 is due to the contribution of the planes (111), (220), and (311) of the zinc-blended ZnS nanocrystals (ICDD PDF 05-0566), which confirms the presence of ZnS with CdS [37]. After core-shell formation, no peak broadening or intensity lowering was observed, which is attributed to the high degree of crystallinity from the presence of the thin ZnS shell, that can preserve the quantum properties of the hexagonal CdS core [38]. Based on the Debye-Scherrer equation, the average particle size for CdS and CdS-ZnS QDs were calculated as 5.5 and 6.2 nm respectively. TiO₂ nanowires (Figure 1c) consists of the anatase phase with diffraction peaks at 25.2, 38, 48.2, 54.4, 63.1, 69.3, and 76.6 (JCPDC 21-1272) [14]. No peaks belonging to any other phase of TiO₂ were detected, indicating the high purity of the synthesized products. After low loading (< 5 weight%) of both types of QDs, the XRD patterns displayed rather weak QD peaks that were more prominent in the case of higher loading. Figure 1 d-e shows bare CdS and core-shell CdS-ZnS QDs (10%) covalently linked with TiO₂ respectively. In both cases, there are additional peaks at 2θ of 28.2, 44, and 52.2, which are attributed to (101), (110), and (112) crystal planes of wurtzite CdS phase and (111), (220), and (311) of the zinc-blended ZnS. The other diffraction peaks of both CdS were not clearly resolved because they overlapped with that of anatase TiO₂. There was no significant change of the anatase TiO₂ peaks after QD loading, resulting from the high crystallinity of the nanocomposite products.

The morphology of both types of QDs were studied using TEM as shown in figures 2a-b. Both samples were present in a dispersed

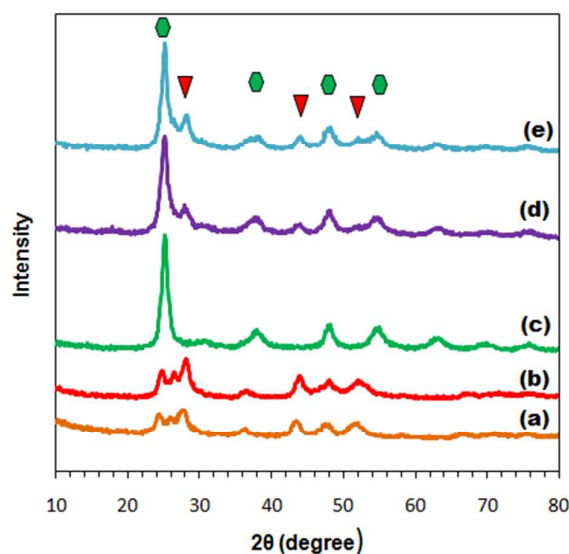


Figure 1. Powder X-ray diffraction pattern: (a) CdS QDs of hexagonal wurtzite, (b) CdS-ZnS core-shell QDs, (c) TiO₂ nanowires after calcination, (d) CdS linked with TiO₂ nanowires, and (e) CdS-ZnS linked with TiO₂ nanowires (green marker presents TiO₂ and red marker QDs).

state, showing formation of individual nanoparticles, although better particle separation was observed after core-shell formation. Here, the thin shell of ZnS minimizes the surface crystal defects and aggregation tendency of CdS. The average particle size was found as 6 ± 1 nm for both bare and core-shell QDs respectively.

As shown in Figure 2c, the TEM image reveals that TiO₂ formed nanowires had an average diameter of 50 nm with a smooth surface. Here, the formation of individual nanowires by inhibiting their agglomeration is due to controlled nanowire growth in the absence of surface tension under supercritical CO₂ [39]. In the case of direct deposition by *in situ* CdS-ZnS QDs synthesis in the presence of TiO₂, QDs were observed agglomerated as seen in Figure 2d. There was also a decrease in nanowire length observed because of vigorous stirring under high temperature during pyrolysis of the QD precursor. Whereas when using MPA linker, the aggregation of nanowires was efficiently overcome and the dispersion of QDs on the TiO₂ surface was improved, which enhanced the interaction between QDs and TiO₂ (Figure 2e-f). This close contact and porous nature of the nanowires is very useful for the electron transfer from QDs to TiO₂, which can potentially limit the recombination of photogenerated electrons and holes [40]. With a closer look at these nanowires (Figure 2 g-h), the dispersed dark and black spots confirms the QDs are bound to the nanowire surface of the TiO₂-QD assembly. The size of these dark spots matches with the size of the CdS and CdS-ZnS QDs. The chemical composition of these spots was further confirmed by SEM-EDX and XPS analysis (described below).

The morphology of the pure TiO₂ and QDs/TiO₂ nanocomposites was also observed by SEM as shown in Figure 3. As is apparent from Figure 3a, the TiO₂ was formed as nanowires, which are 50 nm in diameter and 2-5 μm in length. The surface of the pure TiO₂ nanowires is relatively smooth. Similar to the TEM results, SEM analysis also shows agglomeration of QDs and TiO₂ in the case of

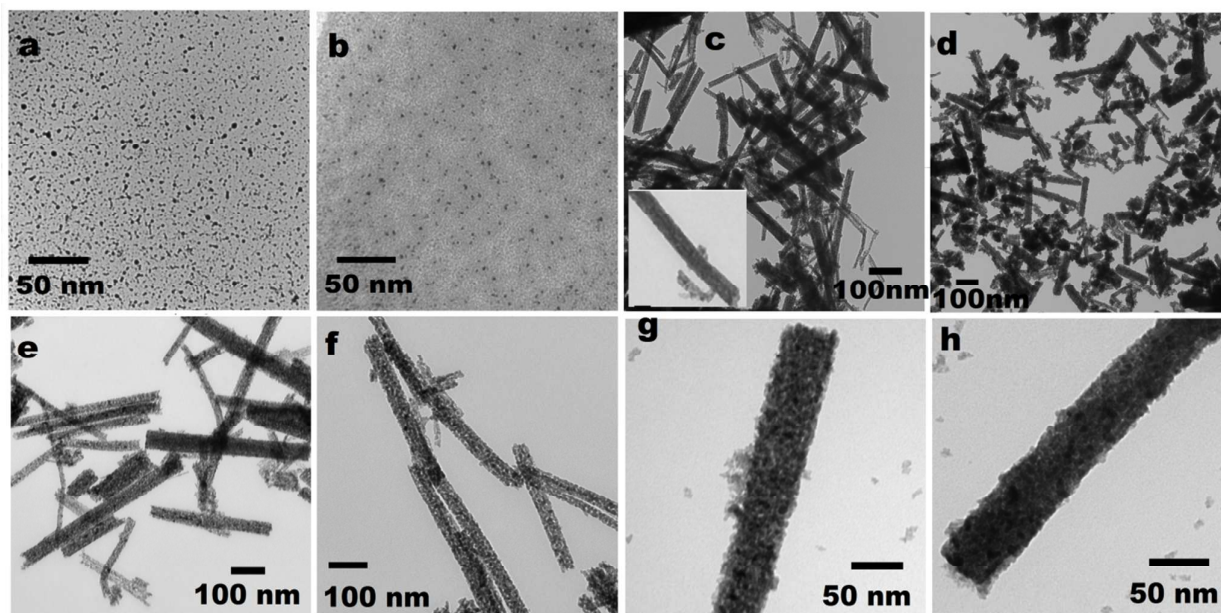


Figure 2. Transmission electron microscopy images of (a) CdS QDs, (b) CdS-ZnS QDs, (c) TiO₂ nanowires prepared under scCO₂, (d) CdS-ZnS direct deposited on TiO₂, (e) CdS linked with TiO₂, (f) CdS-ZnS linked with TiO₂, single TiO₂ nanowire after linking with (g) CdS, and (h) CdS-ZnS QDs.

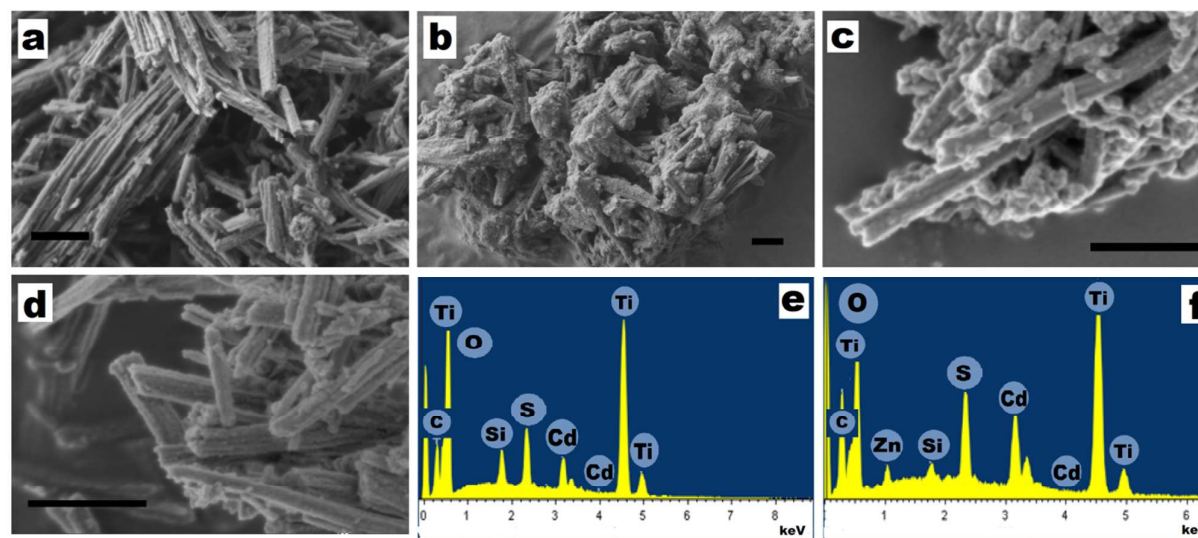


Figure 3. Scanning electron microscopy images of (a) TiO₂ nanowires prepared under scCO₂, (b) CdS-ZnS direct deposited on TiO₂, (c) CdS linked with TiO₂, (d) CdS-ZnS linked with TiO₂, SEM-EDX elemental analysis of (e) CdS linked with TiO₂, and (f) CdS-ZnS linked with TiO₂ [all scale bars indicate 200 nm]

direct deposition (Figure 3b). This agglomeration was effectively reduced after linking of both CdS and CdS-ZnS QDs with TiO₂ nanowires (Figure 3 c-d). In both cases, the surface became quite rough compared to pure TiO₂. The surfaces were analyzed by SEM-EDX, and the results reveal that all the heteroarchitectures are mainly composed of titanium (Ti), oxygen (O), cadmium (Cd), sulfur (S), and zinc (Zn), confirming that the CdS and CdS-ZnS QD particles were successfully loaded onto the TiO₂ nanowires.

During the synthesis of core-shell QDs, a TOA/TOP 2:1 ratio was used that was previously found best to form a thin layer on the QD surface, helping to minimize agglomeration for enhancing optical properties [41]. TOA and TOP are organic and the resulting QDs are hydrophobic in nature [42]. In the case of direct deposition, the QDs are less likely to adsorb to the hydrophilic surface of the TiO₂ nanowires. During the photocatalytic reactions and also washing in the case of cyclic operation, there is a possibility of desorption of these directly deposited QDs from the TiO₂ surface.

However, in the presence of mercaptopropionic acid (MPA), the mercapto end easily adsorbs onto the QD surfaces by replacing the initial surface passivation ligands (TOA/TOP). The carboxylic end of the linker binds with the hydrophilic surface of TiO₂ nanowires [42,43]. Because of the excellent distribution of the QDs on TiO₂ and their better contact (as observed from TEM and SEM analysis), the covalently linked photocatalyst samples are anticipated to show enhanced photocatalytic efficiency than that obtained from direct deposition.

Figure 4 shows the FTIR transmission spectra of free MPA (bifunctional linker), calcined TiO₂ nanowires, and CdS-ZnS QDs linked with TiO₂ nanowires. FTIR was employed to examine whether the -COOH group of MPA was chemically linked to the TiO₂ nanowire surface and if the -SH group was chemically bonded to the QD surface. In the case of TiO₂, the band at about 1617 cm⁻¹ corresponding to the bending vibration of H-O, and the broad band starting from 900 cm⁻¹ is assigned to the stretching of Ti-O-Ti [10]. Free MPA provides strong bands at 1698 and 1424 cm⁻¹, are typical for the asymmetric C=O and symmetric C-O stretching peaks of carboxylate (Figure 4a). The 2500-2600 cm⁻¹ band corresponds to the -SH group and a broad band in the range 2800-3200 cm⁻¹ is attributed to the O-H band of MPA [14]. The FTIR spectra of bare TiO₂ was modified after linking CdS-ZnS QDs through the bifunctional linker MPA, as shown in Figure 4b. There are at least three significant changes between free MPA and QDs-MPA-TiO₂; (1) there is no C=O peak for QDs-MPA-TiO₂ at 1698 cm⁻¹, however, at

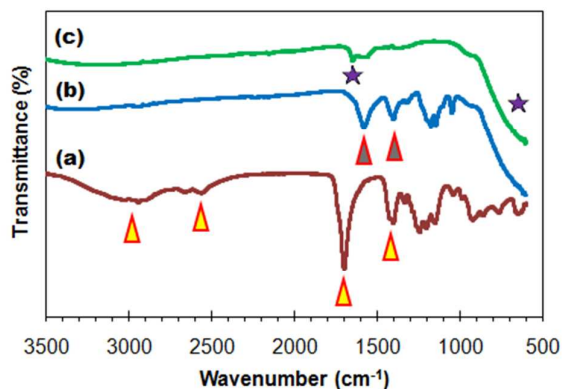


Figure 4. FTIR spectra of (a) 3-Mercaptopropionic acid (MPA), (b) CdS-ZnS QDs - MPA-TiO₂, and (c) TiO₂ nanowires prepared under supercritical CO₂ and calcined at 450°C.

the multiple carboxylate region (1510-1655 cm⁻¹), a well-resolved band at 1584 cm⁻¹ is evolved; (2) the broad O-H band of carboxylate at 2800-3200 cm⁻¹ is absent for QDs-MPA-TiO₂; (3) there is no -SH group peak at 2500-2600 cm⁻¹. The first two changes provide clear evidence for the attachment of the -COOH group of MPA to the TiO₂ surface, and the third change indicates the absence of the free

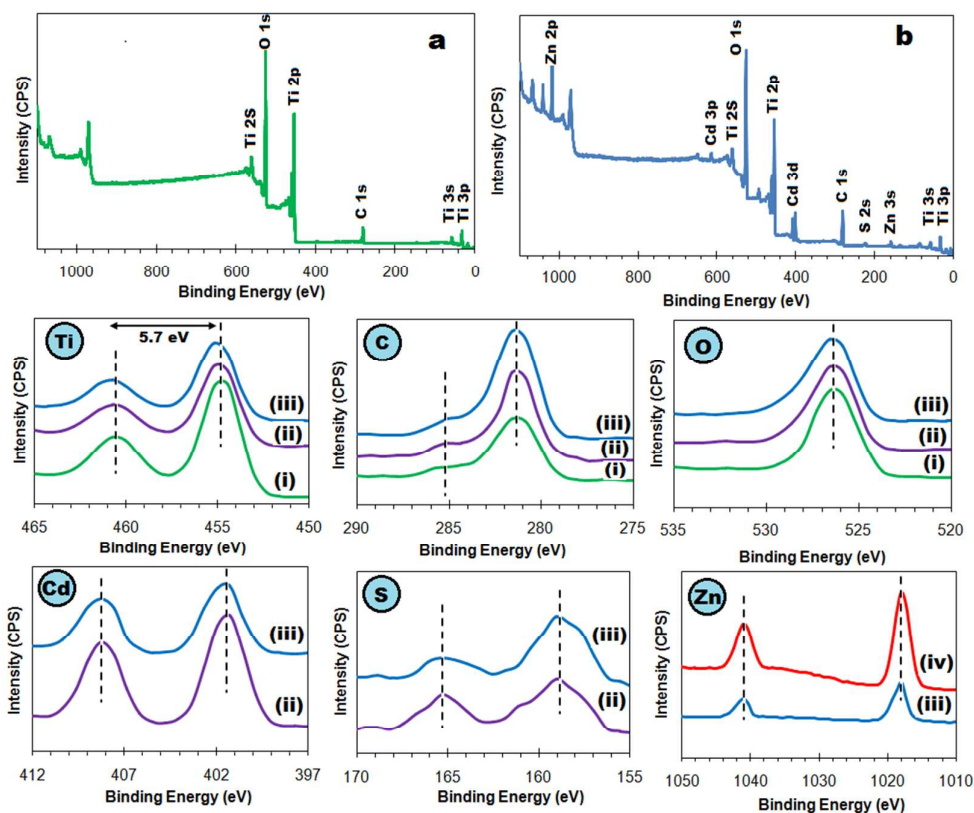


Figure 5. X-ray photoelectron spectroscopy (XPS) survey scan of (a) TiO₂ nanowires, (b) CdS-ZnS QDs linked with TiO₂ nanowires; high resolution XPS spectra of the principal elements Ti 2p, C 1s, O 1s, Cd 3d, S 2p and Zn 2p for samples (i) TiO₂ nanowires, (ii) CdS QDs linked with TiO₂ nanowires, (iii) CdS-ZnS linked with TiO₂ nanowires, and (iv) CdS-ZnS QDs.

mercapto groups and the formation of robust bonding between QD and MPA [14].

XPS was carried out to further investigate QD nanoparticles linking to TiO₂, the chemical composition of the nanocomposites and the valence state of various species present therein. The full survey scan over a large energy range at low resolution indicates the presence of Ti, O, and C in TiO₂ (Figure 5a), and Ti, O, C, Cd, Zn, and S in CdS-ZnS QDs linked with TiO₂ (Figure 5b). In the high resolution XPS spectra it is clearly seen that, the spin-orbit components (2p_{3/2} and 2p_{1/2}) of the Ti 2p peak were deconvoluted into two curves at 454.7 and 460.4 eV, corresponding to Ti⁴⁺ in a tetragonal structure. The measured separation between these two peaks was 5.7 eV, which is consistent with the binding energy separation observed for stoichiometric TiO₂ [6]. After both bare CdS and core-shell CdS-ZnS QDs linking with TiO₂, both these peaks exhibited a slight shift due to chemical attachment of QDs with TiO₂ through the linker and transferring the electrons from QDs into the TiO₂ lattice [29]. However, in both cases the separation of the peaks remained as 5.7 eV, confirming the high quality of TiO₂ after QD loading. The C 1s spectrum exhibits two peaks located at 281.2 and 285.2 eV corresponding to C-H and C-O respectively. For bare TiO₂, hydrocarbon is related to the residual carbon coming from the decomposition of the titanium precursor and some surface contaminants during XPS analysis [44]. But the intensity of the same peak was increased after QD loading because of additional hydrocarbon from the linker molecule. The peak of C-O at 285.2 eV, and absence of any peak for C=O and O-C=O (at 288-290 eV) confirms the successful attachment of the linker with the TiO₂ surface. Similarly, the O 1s shows a major peak at 526.3 eV attributed to crystal lattice oxygen (O_{Ti-O}). There was no peak for surface hydroxyl group (O_{O-H}) at around 530 eV was observed. In the photoelectron spectrum of Cd 3d, the peaks at 401.5 and 408.2 eV are assigned for Cd 3d_{5/2} and 3d_{3/2} respectively. The spin-orbit separation of these peaks is 6.7 eV, which corresponds to the presence of the oxidation state +2 of Cd at the surface [6]. The S 2p core level spectrum indicates the significant peak at 159 eV corresponding to S²⁻ of QDs. The presence of other peaks at 165.2 eV is due to the formation of S-S bond between the linker and the QDs [37]. The Zn 2p core-level XPS spectrum of CdS-ZnS QDs before and after linked with TiO₂ showed the doublet spectral lines at 1018 eV (Zn 2p_{3/2}) and 1041 eV (Zn 2p_{1/2}) with a spin-orbit separation of 23 eV, which corresponds to the Zn²⁺ oxidation state and is in good agreement with the previously published value of ZnS [45]. The results of the XPS measurement, together with FTIR analysis and SEM-EDX measurement suggests that both QDs were successfully loaded and linked with TiO₂ nanowires.

3.2 Optical properties

The UV-visible spectrum was examined to evaluate the optical response of TiO₂ nanowires after loading CdS-ZnS QDs, with and without linker, and also changing the concentration of QDs in TiO₂. It can be seen that the bare TiO₂ nanowires exhibit a fundamental sharp absorption edge at approximately 387 nm, with no significant absorption for visible light (Figure 6a). The band gap energy was measured by drawing a tangent line on the edge of the spectra to determine the cut off wavelength at $y=0$ [4]. The band gap energy

for the bare TiO₂ was estimated as 3.2 eV, that matches with pure anatase TiO₂ [39]. CdS-ZnS QDs showed a broad and continuous excitation spectrum in the UV range and lower wavelength visible range with corresponding absorption edges at 510 nm and a band gap energy 2.5 eV, as shown in Figure 6a (line iv). TiO₂ nanowires loaded with CdS-ZnS QDs exhibit enhanced and broad absorption both in the UV and visible regions, indicating the effective combination of the absorption properties of TiO₂ and QDs in the UV region and QDs in the visible region. There was a blue shift of the absorption edge observed in the case of nanocomposites prepared using MPA linker compared to that for nanocomposites without linker (direct deposition). The reason behind this blue shift is the attachment of CdS-ZnS QDs onto the TiO₂ surface via the studied linker molecule [46]. A similar blue shift has also been observed for a similar linker for other types of QDs [14], Si-O-Cd covalent linkage in CdS-SiO₂ [47], and Ti-O-C bonding in TiO₂ with graphene [29]. The composites using a linker exhibited much stronger light absorbance in the visible range than those prepared by direct deposition. This higher absorption is attributed to both the excellent dispersion of CdS-ZnS QDs onto the TiO₂ surface and the strong covalent linkage between QDs and TiO₂ [39].

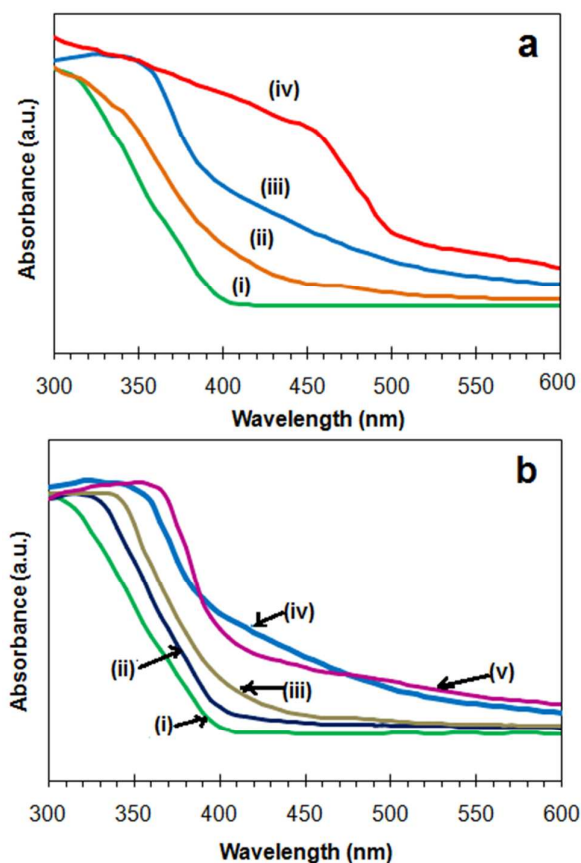


Figure 6. UV-Vis absorption spectra of: (a) effect of linker: (i) TiO₂ nanowires synthesized under supercritical CO₂, (ii) CdS-ZnS QDs loaded TiO₂ via direct deposition, (iii) CdS-ZnS QDs loaded TiO₂ via linker, (iv) CdS-ZnS QDs; (b) effect of loading concentration: (i) TiO₂ nanowires, and CdS-ZnS QDs loaded TiO₂ via linker with QDs loading (weight %): (ii) 2%, (iii) 5%, (iv) 10%, and (v) 20%.

As shown in Figure 6b, the absorption intensity in the region 400–510 nm was increased with the increase of CdS-ZnS QDs linking to TiO₂. For the lower loading (< 5%), there was only a small change in the intensity, however in the case of 10% loading a stronger absorbance was observed in that region. With a further increase of QD loading, there was no significant change in the intensity, which can be attributed to the aggregation of QDs that causes non-radiative light emission, and also the crystal growth of QDs, leading to poor photo-sensitization [39]. It was also observed that with more than 10% loading, TiO₂ loses its hydrophilicity nature, which will reduce the dispersion ability of those nanocatalysts in the aqueous solution of organic dye/pollutants during the photocatalytic activity study.

Although aqueous synthesis of QDs is convenient, the quality and stability of the QDs are better when synthesized in organic solution [42]. TOA/TOP capped QDs remain highly dispersible in organic solvents such as toluene and chloroform, and a stable photoluminescence was observed after two months for the samples kept under dark and at room temperature (data not shown). We have previously reported that, compared to a fluorescent dye, CdS QDs can minimize photobleaching by 70% under continuous exposure of excited UV light [32]. In addition, a thin layer of ZnS on the CdS QDs further enhances the photostability, as the ZnS shell suppresses the photochemical degradation of CdS, protecting the exciton wavefunction from nonradiative recombination processes as surface traps [48]. When the QDs are attached with a linker or ligand, the optical properties and stability are often improved [33]. Therefore, it is anticipated that linking with MPA and loaded onto TiO₂ nanowires enhances the photostability of both the core CdS and core-shell CdS-ZnS QDs.

3.3 Photocatalytic performance

Photocatalytic activities of the CdS/TiO₂ and CdS-ZnS/TiO₂ heteroarchitectures with different amounts of QDs, with and without linker, and bare TiO₂ nanowires were verified through investigating the photo-degradation of methylene blue (MB) in aqueous solution under both UV and visible light irradiation. A decrease in sample absorbance at maximum wavelength for MB (664 nm) indicates degradation of MB. Both the blank experiments (i) with photocatalyst in the absence of irradiation and (ii) without photocatalyst in the presence of irradiation, were carried out to rationalize the photocatalytic activity of the synthesized photocatalysts. The degradation efficiency of the experimental photocatalysts was defined as C/Co , where Co is the initial concentration of MB after equilibrium adsorption, and C is the concentration at defined intervals during the experiment. Blank experimental results showed that MB could not be decomposed under dark even in the presence of the photocatalyst (Figure 7 a-b). The degradation of MB under light in the absence of photocatalysts is much slower, so that the impact of self-degradation could be ignored. Under UV irradiation as shown in Figure 7a, the synthesized TiO₂ nanowires with and without loading of both CdS and CdS-ZnS QDs showed strong degradation efficiency. This is because both the TiO₂ and QDs exhibit very high absorption in the UV region as shown earlier (Figure 6). The degradation efficiency of the TiO₂ nanowires was more than 50% after the first 40 min, that was increased after QDs loading. The QD nanoparticles loaded on the TiO₂ nanowires act as the separation centres of electrons and holes, thereby improving the photocatalytic efficiency [6]. Compared to the direct deposition, covalent linking of QDs onto TiO₂ nanowires showed better efficiency because of excellent

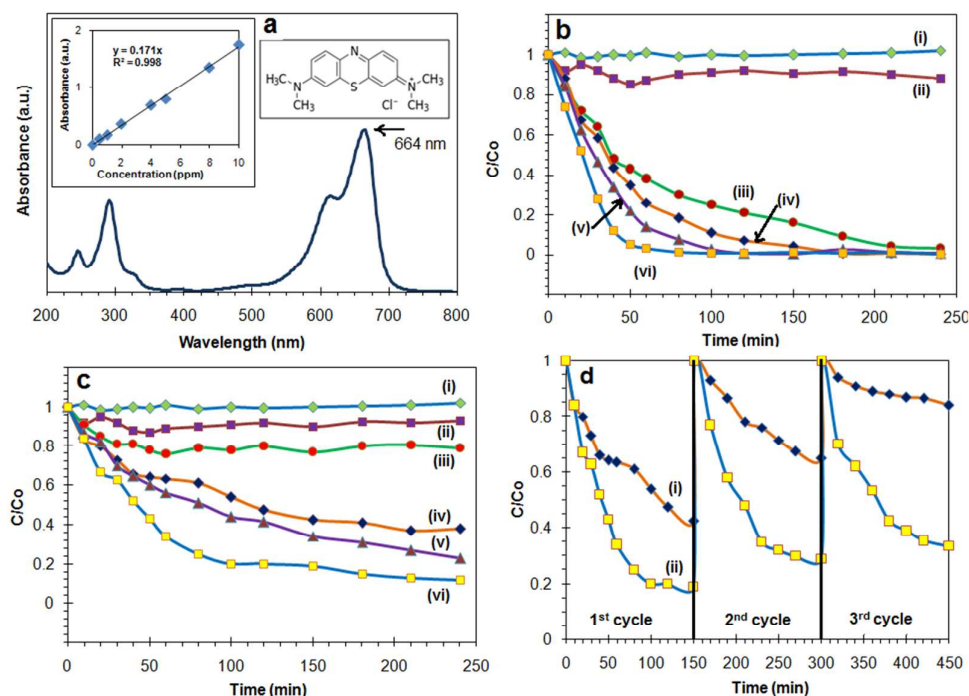


Figure 7. (a) UV-visible absorption spectrum, calibration curve, and molecular structure of methylene blue (MB) dye; photocatalytic degradation of MB under (b) UV only, (c) visible solar irradiation (>365 nm), in both cases (i) CdSZnS-MPA-TiO₂ + MB under dark, (ii) MB under irradiation, (iii) TiO₂ + MB, (iv) direct deposited CdSZnS-TiO₂ + MB, (v) CdS-MPA-TiO₂ + MB, (vi) CdSZnS-MPA-TiO₂ + MB; (d) cyclic runs in the photodegradation of MB using (i) direct deposited CdSZnS-TiO₂, (ii) CdSZnS-MPA-TiO₂ [QDs loading on TiO₂ = 10%]

distribution of the QDs on TiO₂ and superior contact between them as observed from SEM and TEM analysis (Figure 2 & 3).

Between bare CdS and core-shell CdS-ZnS QDs, core-shell QDs linked on TiO₂ nanowires showed higher efficiency (88% compared to 64% in first 40 min). We previously reported that the thin ZnS shell helps to minimize any surface crystal defects and decrease the aggregation tendency of the bare CdS QDs, providing uniform dispersion and increasing the quantum yield from 25% to 48% [23]. In contrast, under artificial solar irradiation (> 365 nm), bare TiO₂ exhibited a very small activity up to 15% photo-degradation of MB (Figure 7b), mainly because of the absorption in the region 365–400nm. CdS-ZnS QDs-MPA-TiO₂ showed the highest MB decomposition under both visible and UV irradiation. After 180 min, 85% of MB was degraded with this photocatalyst, whereas 70 and 59% was decomposed by CdS-MPA-TiO₂ and CdS-ZnS-TiO₂ respectively. This result shows that both the UV and visible light induced catalytic efficiency of TiO₂ nanowires was significantly enhanced by QDs linking, especially core-shell QDs than bare QDs.

In addition, the synthesized photocatalysts can be recycled and reused several times without a significant loss of efficiency, which is a key requirement for large scale application [49]. In the case of direct deposited CdS-ZnS QDs onto TiO₂ nanowires, after the first cycle there was more than 50% decomposition of MB observed, whereas this efficiency decreased significantly after the second and third cycles to 35 and 16 % respectively. This reduction of efficiency is attributed to detachment of QDs from TiO₂ surfaces during photocatalytic reaction and washing. In contrast, the covalently attached CdS-ZnS QDs on TiO₂ nanowires showed only 10% lowering of efficiency after the first cycle, and any further decrease is negligible after the second cycle. Therefore, the core-shell QDs linked with TiO₂ nanowires not only exhibits very good photocatalytic activity but also high stability. Similar observations have been reported earlier for CdS linked with TiO₂ nanofibers [14], CdS-graphene-TiO₂ nanotubes [50] and graphene modified nano-Ag₃PO₄ [51].

For a better comparison of the photocatalytic activities of the experimental samples with different loading concentration of both types of QDs, the reaction kinetics were calculated based on Langmuir-Hinshelwood model, which can be expressed as [4];

$$-\frac{dC}{dt} = k_t \frac{K_a C}{1 + K_a C} \quad (1)$$

where (-dC/dt) is the degradation rate of MB, C is the concentration of MB in the solution at a reaction time of t, k_t is the reaction rate constant, and K_a is the adsorption coefficient of the reactant. K_a C is negligible when the initial concentration of MB is very low. As a result equation (1) can be described as pseudo-first order kinetics. Setting equation (1) at the initial conditions, when t=0, C=C₀, it can be described as;

$$\ln \frac{C}{C_0} = -k_{app} t \quad (2)$$

where k_{app} is the apparent rate constant, that can be obtained from the plot of the experimental data.

Photocatalytic degradation of dyes generally follows pseudo-first order kinetics [52]. The apparent rate constant of different experimental photocatalysts for the fixed initial dye concentration

and catalyst concentration are indicated in Table 1. For the bare TiO₂ nanowire, the value of k_{app} was minimum both under UV (0.017 min⁻¹) and visible (0.002 min⁻¹) lights. However, after QD loading, a significant enhancement of the k_{app} value was observed especially under visible solar irradiation. It was observed that the photocatalytic activity is governed by QD loading onto TiO₂ nanowires and also the mode of attachment between QDs and TiO₂. The results show that the rate of dye degradation increases with an increase of QD loading from 2 to 10%. In explanation, QDs produce more OH• radicals, which are active oxidative species causing photodegradation of MB. At the same time, the QDs increase UV absorption, as well as extending the absorption to the visible range, while also helping to separate electrons and holes, thereby improving photodegradation of MB. Higher levels of loading favour the recombination of electrons and holes, leading to a lowering of photocatalytic efficiency [6]. According to the experimental kinetic data, 10% loading of CdS-ZnS QDs linked with TiO₂ nanowires exhibited the highest efficiency for MB degradation. Further increasing of QD loading causes aggregation of QDs as described earlier, leading to poor optical properties and photo-sensitization. The apparent kinetic rate constant was also increased in the case of QDs linked with TiO₂ compared to those prepared by direct deposition. The reason behind this, the linker molecule efficiently helps to overcome the aggregation of nanowires, improving the dispersion of QDs on TiO₂, resulting in enhanced interaction between QDs and TiO₂ as shown earlier by SEM and TEM analysis.

Table 1. Apparent rate constants for the degradation of methylene blue (MB) with synthesized TiO₂ nanowires direct deposition and linking with different loading of bare and core-shell QDs.

Photocatalysts	k _{app} (min ⁻¹) (UV)	k _{app} (min ⁻¹) (visible)
TiO ₂ nanowire	0.017	0.002
CdSZnS-MPA-TiO ₂ 2%	0.016	0.006
CdSZnS-MPA-TiO ₂ 5%	0.034	0.011
CdSZnS-MPA-TiO ₂ 10%	0.052	0.016
CdSZnS-MPA-TiO ₂ 20%	0.041	0.013
CdS-MPA-TiO ₂ 10%	0.027	0.009
CdSZnS-TiO ₂ Direct deposition	0.020	0.007

Instead of using direct sunlight due to the large variation of UV levels [53], the photocatalytic degradation of dyes was investigated under simulated solar light (without using a UV cut off filter) for two intensities 14 and 28 mW/cm² and variable catalyst loading concentrations. These results were then compared with the photocatalytic efficiencies observed under UV and visible light separately. Under both intensities, MB dyes did not show any degradation in the absence of the photocatalyst (Figure 8a). The results show that the UV intensity of solar light plays an important role in the degradation of MB. At 28 mW/cm² for 1.2g/L catalyst loading, MB was decomposed completely within one hour. Increasing the UV intensity provides more energy to excite the electrons of TiO₂ and QDs, creating more electron-hole pairs and also producing more OH• radicals, thus enhances the photocatalytic process [52]. The rate constant and half life at 14 mW/cm² were calculated as 0.024 min⁻¹ and 28.87 min respectively (Figure 8b). The half life under only UV and visible light were 13.3 and 43.3 min respectively. It is observed that compared to only visible light, the rate constant of the degradation reaction was relatively higher and the half life of the reaction was less under simulated sunlight, which leads to the faster degradation of MB under sunlight. In the case of photodegradation of MB under UV and visible only light, a higher catalyst loading concentration (1.2 g/L) was used for faster

photodegradation, as the increasing catalyst concentration will provide more active sites. For anatase TiO_2 catalyst, a critical catalyst loading of 2 g/L has been described [54]. At a concentration lower than this value, k_{app} increases with increasing catalyst concentration. Some research groups have reported catalyst loading concentrations of 1.2 g/L or higher for the decomposition of similar initial concentration of dyes [39,51,55].

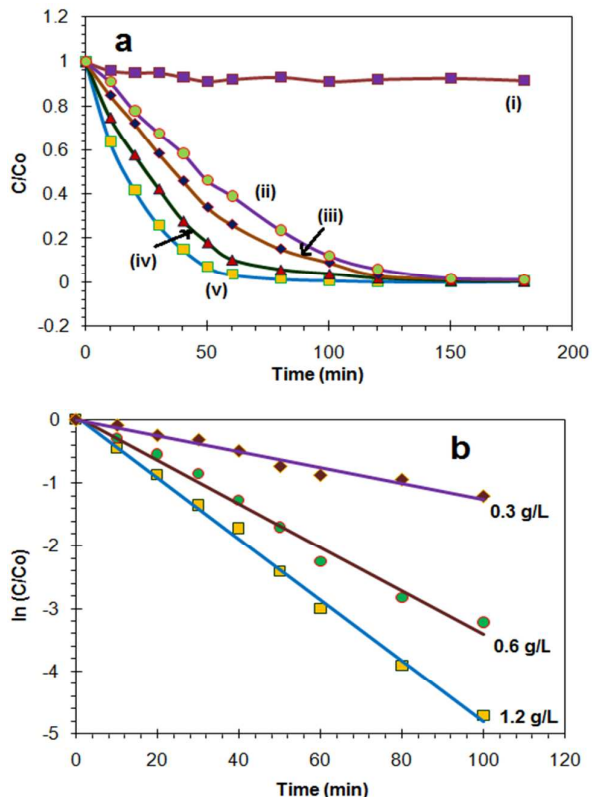


Figure 8. photocatalytic degradation of methylene blue (MB) dye by CdSZnS-MPA-TiO_2 nanowires under simulated solar lights (without cut off filter) and the effect of UV intensity and catalyst dosage; (a) photocatalytic activity; (i) MB only at 28 mW/cm^2 , (ii) 14 mW/cm^2 , 0.6 g/L, (iii) 14 mW/cm^2 , 1.2 g/L, (iv) 28 mW/cm^2 , 0.6 g/L, (v) 28 mW/cm^2 , 1.2 g/L; (b) $\ln(C/C_0)$ as a function of the irradiation time for changing catalyst loading concentration of CdSZnS-MPA-TiO_2 nanowires [initial MB concentration: 10 mg/L].

In addition, the photocatalytic degradation of MB was also studied with changing catalyst (CdSZnS-MPA-TiO_2 nanowires) loading concentration under stimulated solar light as shown in Figure 8b. For the lowest concentration (0.3 g/L), the apparent rate constant was 0.012 min^{-1} , and 70% of dye was decomposed in the first 2 hours. By further increasing the concentration to 0.6 g/L, 100% dye decomposition was observed in the first 2 hours with a k_{app} 0.033 min^{-1} . For the highest dosage 1.2 g/L, the decomposition was very fast with a rate constant 0.047 min^{-1} . In considering the process economy, 0.6 g/L would be an optimum loading concentration as it shows a high photocatalytic degradation of MB dye in a reasonable time period.

Figure 9 provides the OH^\bullet production by the experimental photocatalyst (CdSZnS-MPA-TiO_2 nanowires) with terephthalic acid

as a fluorescent probe. No peak was observed in the absence of light or photocatalyst samples. But in the presence of light, a gradual increase in PL intensity at about 425 nm was observed with increasing irradiation time (from 5 to 30 min). This has been shown to be from the formation of highly fluorescent product, 2-hydroxyterephthalic acid from the reaction of terephthalic acid and OH^\bullet [51,56]. Higher intensities indicate higher amounts of OH^\bullet production, which is the major species responsible for the photocatalytic degradation of MB.

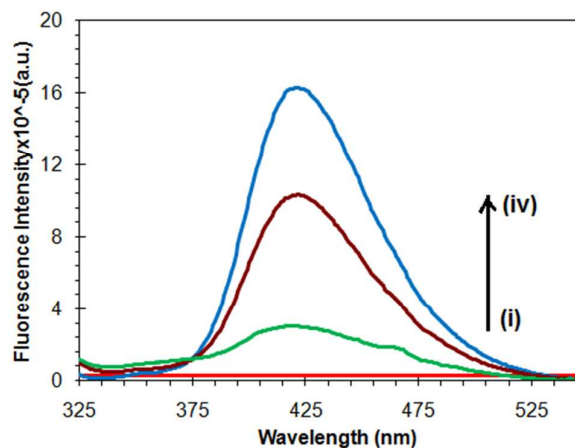
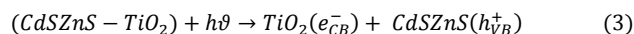


Figure 9. Photoluminescence spectral changes observed during UV irradiation of the CdSZnS-MPA-TiO_2 in a basic solution of terephthalic acid at (i) before irradiation, (ii) 5 min, (iii) 15 min, (iv) 30 min (excitation wavelength 315 nm).

A proposed mechanism of excitation and charge transfer process between the core-shell CdS-ZnS QDs and TiO_2 is shown in Figure 10. In this work, we fabricated CdS-ZnS QDs for broad absorption and efficient carrier extraction in TiO_2 assemblies. Due to the position of the conduction band (CB) and valence band (VB) of both QDs, the optimal CB and VB edges are located in the core CdS QDs. The electron-hole recombination rate is much slower in the core-shell QDs than that of the core QDs because of instability of the core [57]. As the CB edge of TiO_2 is more positive than this optimal CB of the core-shell QDs, the photogenerated electrons are transferred to the CB of TiO_2 , leading to a higher concentration of electrons. Meanwhile, the hole generated on the optimal VB of QDs remains instead of being transferred to the VB of TiO_2 , as this optimal VB is more cathodic than that of TiO_2 [58].

The electrons (e^-) accumulated at the CB of TiO_2 are scavenged by dissolved oxygen molecules in water to yield superoxide radical anions ($\text{O}_2^{\bullet-}$) (equation 4), yielding hydroperoxy radicals HO_2^\bullet on protonation (equation 6), and finally hydroxyl radicals OH^\bullet (equation 7). During this reaction, H_2O_2 is also formed which can be further reduced to OH^\bullet (equation 8). Meanwhile, the holes on the optimal VB of the core-shell QDs can potentially react with surface hydroxyl groups or physisorbed water molecules to form OH^\bullet radicals (equation 5). The highly reactive OH^\bullet radicals are strong oxidising agents which can decompose organic pollutants [46, 47]. The proposed mechanism illustrated in Figure 10 can be summarized as the following equations:



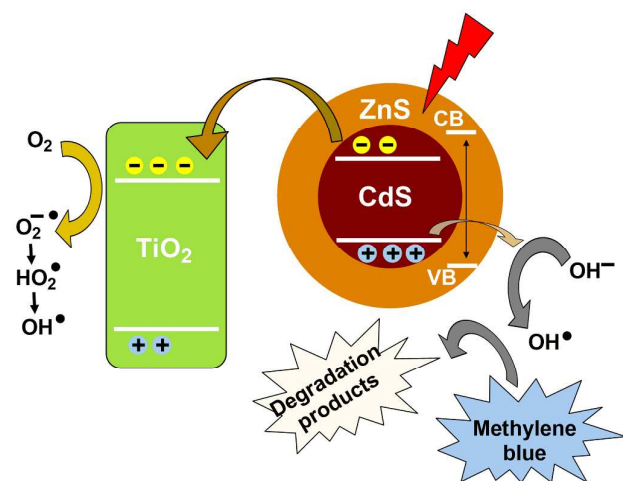
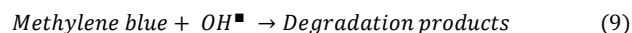
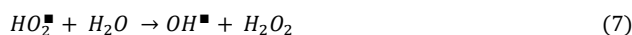
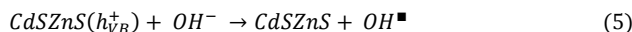
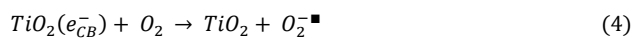


Figure 10. Schematic description of the charge transfer and separation between CdS-ZnS and TiO₂ in the CdS-ZnS QDs linked with TiO₂ nanowires under visible irradiation.

Conclusions

A new methodology was developed to efficiently link core-shell CdS-ZnS QDs to porous TiO₂ nanowires by using an abundant bifunctional linker, MPA. The core-shell QDs were synthesized based on pyrolysis of a single-molecule precursor method. The thin layer of ZnS grown on CdS core, inhibits the photocorrosion and passivates the trap states on CdS QDs, enhancing the photoluminescence and quantum yield. High quality anatase TiO₂ nanowires were prepared using a sol-gel technique in scCO₂. The morphology and distribution of QDs on the TiO₂ surface was confirmed by XRD, TEM, SEM, and XPS. The FTIR and XPS results also confirmed the successful linking between QDs and TiO₂. UV-visible absorption analysis showed that strong interactions using the linked QDs and loading concentration played a key role to enhance lower wavelength visible light absorption of TiO₂ nanowires. CdS-ZnS QDs linked with TiO₂ showed the highest activity for photodecomposition of methylene blue with 10% QD loading. This study also showed that core-shell structure of QDs and covalent linking is important for both activity and stability of heterogeneous photocatalysts. This novel semiconducting

heterojunction nanocatalyst with high photocatalytic activity and stability can be potentially applicable for removing undesirable organics from the environment.

Acknowledgements

This work was financially supported by the Canadian Natural Science and Engineering Research Council (NSERC) Discovery Program, Western University and MITACS-accelerate Program, Canada. Authors also thank to Patrick Therrien and Jeremy van Esbroeck of Sunwash Technologies, Canada for fruitful discussion and help during simulated solar light experiments.

References

- 1 R. Dagherir, P. Drogui, D. Robert, *Industrial & Engineering Chemistry Research*, 2013, **52**, 3581.
- 2 S.G. Kumar, L.G. Devi, *The Journal of Physical Chemistry A*, 2011, **115**, 13211.
- 3 P. Roy, D. Kim, K. Lee, E. Spiecker, P. Schmuki, *Nanoscale*, 2010, **2**, 45.
- 4 N. Farhangi, R.R. Chowdhury, Y. Medina-Gonzalez, M.B. Ray, P.A. Charpentier, *Applied Catalysis B: Environmental*, 2011, **110**, 25.
- 5 M.D. Hernández-Alonso, F. Fresno, S. Suárez, J.M. Coronado, *Energy & Environmental Science*, 2009, **2**, 1231.
- 6 C. Su, C. Shao, Y. Liu, *Journal of Colloid and Interface Science*, 2011, **359**, 220.
- 7 Y. Medina-Gonzalez, W.Z. Xu, B. Chen, N. Farhanghi, P.A. Charpentier, *Nanotechnology*, 2011, **22**, 065603.
- 8 G.-S. Li, D.-Q. Zhang, J.C. Yu, *Environmental Science & Technology*, 2009 **43**, 7079.
- 9 L. Yang, S. Luo, R. Liu, Q. Cai, Y. Xiao, S. Liu, F. Su, L. Wen, *The Journal of Physical Chemistry C*, 2010, **114**, 4783.
- 10 P. Thakur, R. Chadha, N. Biswas, S.K. Sarkar, T. Mukherjee, S.S. Joshi, S. Kapoor, *Materials Research Bulletin*, 2012, **47**, 1719.
- 11 M. Feng, H. Zhan, L. Miao, *ACS Applied Materials & Interfaces*, 2010, **2**, 1129.
- 12 A. Pareek, R. Purbia, P. Paik, N.Y. Hebalkar, H.G. Kim, P.H. Borse, *International Journal of Hydrogen Energy*, 2014, **39**, 4170.
- 13 S.K. Arya, T. Vats, S. Sharma, K. Singh, A.K. Narula, *Journal of Thermal Analysis and Calorimetry*, 2012, **107**, 555.
- 14 S. Qian, C. Wang, W. Liu, Y. Zhu, W. Yao, X. Lu, *Journal of Materials Chemistry*, 2011, **21**, 4945.
- 15 N. Guijarro, T. Lana-Villarreal, I. Mora-Seró, J. Bisquert, R. Gómez, *The Journal of Physical Chemistry C*, 2009, **113**, 4208.
- 16 D.R. Pernik, K. Tvrđy, J.G. Radich, P.V. Kamat, *The Journal of Physical Chemistry C*, 2011, **115**, 13511.
- 17 N. Ghows, M.H. Entezari, *Ultrasonics Sonochemistry*, 2012, **19**, 1070.
- 18 M. Darbandi, G. Urban, M. Krüger, *Journal of Colloid and Interface Science*, 2010, **351**, 30.
- 19 M.N. Bahrami, K. Rezaee, M. Zobir, *Chalcogenide Letters*, 2012, **9**, 379.
- 20 C. V. Durgadas, K. Sreenivasan, C.P. Sharma, *Biomaterials*, 2012, **33**, 6420.
- 21 D. Bera, L. Qian, T.-K. Tseng, P.H. Holloway, *Materials*, 2010, **3**, 2260.
- 22 H. Chen, W. Li, H. Liu, L. Zhu, *Microporous and Mesoporous Materials*, 2011, **138**, 235.
- 23 M.A. Mumin, K.F. Akhter, P.A. Charpentier, *AIP Conference*

- Proceedings*, 2014, **1590**, 259.
- 24 P. A. Charpentier, W. Z. Xu, X. Li, *Green Chemistry*, 2007, **9**, 768.
- 25 R. Sui, P.A. Charpentier, *Chemical Reviews*, 2012, **112**, 3057.
- 26 N. Farhangi, S. Ayissi, P.A. Charpentier, *Nanotechnology*, 2014, **25**, 305601.
- 27 R. Sui, A.S. Rizkalla, P.A. Charpentier, *The Journal of Physical Chemistry B*, 2006, **110**, 16212.
- 28 R. Sui, A.S. Rizkalla, P.A. Charpentier, *Microporous and Mesoporous Materials*, 2011, **142**, 688.
- 29 A.I. Copper, *Advanced Materials*, 2003, **15**, 1049.
- 30 T. Luttrell, S. Halpegamage, J. Tao, A. Kramer, E. Sutter, M. Batzill, *Scientific Reports*, 2014, **4**, 4043.
- 31 J. Zhang, P. Zhou, J. Liu, J. Yu, *Physical Chemistry Chemical Physics*, 2014, **16**, 20382.
- 32 M.A. Mumin, W.Z. Xu, P.A. Charpentier, *Nanotechnology*, 2015, **26**, 315702.
- 33 J.M. Allan, M.A. Mumin, W.Z. Xu, Q. Al Sharari, P.A. Charpentier, *Solar Energy Materials and Solar Cells*, 2014, **123**, 30.
- 34 K. Ishibashi, A. Fujishima, T. Watanabe, K. Hasimoto, *Journal of Photochemistry and Photobiology A: Chemistry*, 2000, **134**, 139.
- 35 K. Ishibashi, A. Fujishima, T. Watanabe, K. Hasimoto, *Electrochemistry Communications*, 2000, **2**, 207.
- 36 K. Park, H.J. Yu, W.K. Chung, B.-J. Kim, S.H. Kim, *Journal of Materials Science*, 2009, **44**, 4315.
- 37 J. Liu, Z. Guo, W. Wang, Q. Huang, K. Zhu, X. Chen, *Nanoscale*, 2011, **3**, 1470.
- 38 M. Bruchez, M. Moronne, P. Gin, S. Weiss, A.P. Alivisatos, *Science*, 1998, **281**, 2013.
- 39 Y. Huo, X. Yang, J. Zhu, H. Li, *Applied Catalysis B: Environmental*, 2011, **106**, 69.
- 40 D. He, M. Chen, F. Teng, G. Li, H. Shi, J. Wang, M. Xu, T. Lu, X. Ji, Y. Lv, *Superlattices and Microstructures*, 2012, **51**, 799.
- 41 W.Z. Xu, P.A. Charpentier, *The Journal of Physical Chemistry C*, 2009, **113**, 6859.
- 42 T.J. Macdonald, T. Nann, *Nanomaterials*, 2011, **1**, 79.
- 43 H. Zhu, M.Z. Hu, L. Shao, K. Yu, R. Dabestani, M.B. Zaman, S. Liao, *Journal of Nanomaterials*, 2014, **324972**, 1.
- 44 M.N. Ghazzal, R. Wojcieszak, G. Raj, E.M. Gaigneaux, *Beilstein Journal of Nanotechnology*, 2014, **5**, 68.
- 45 Z.H. Ibupoto, K. Khun, X. Liu, M. Willander, *Nanomaterials*, 2013, **3**, 564.
- 46 J. C. Kim, J. Choi, Y.B. Lee, J.H. Hong, J.I. Lee, J.W. Yang, W.I. Lee, N.H. Hur, *Chemical Communications*, 2006, 5024.
- 47 H. Weib, A. Fernandez, H. Kisch, *Angewandte Chemie International Edition*, 2011, **40**, 3825.
- 48 T. Jamieson, R. Bakhshi, D. Petrova, R. Pocock, M. Imani, A.M. Seifalian, *Biomaterials*, 2007, **28**, 4717.
- 49 M.T. Uddin, Y. Nicolas, C.I. Olivier, T. Toupance, L. Servant, M.M. Müller, H.-J. Kleebe, J. Ziegler, W. Jaegermann, *Inorganic Chemistry*, 2012, **51**, 7764.
- 50 J. Xian, D. Li, J. Chen, X. Li, M. He, Y. Shao, L. Yu, J. Fang, *ACS Applied Materials & Interfaces*, 2014, **6**, 13157.
- 51 Q. Xiang, D. Lang, T. Shen, F. Liu, *Applied Catalysis B: Environmental*, 2015, **162**, 196.
- 52 M. Salehi, H. Hashemipour, M. Mirzaee, *American Journal of Environmental Engineering*, 2012, **2**, 1.
- 53 V.E. Fioletov, M.G. Kimlin, N. Krotkov, L.J.B. McArthur, J.B. Kerr, D.I. Wardle, J.R. Herman, R. Meltzer, T.W. Mathews, J. Kaurola, *Journal of Geophysical Research*, 2004, **109**, 22308.
- 54 E.I. Kapinus, T.I. Viktorova, *Theoretical and Experimental Chemistry*, 2010, **46**, 163.
- 55 J. Pan, Y. Sheng, J. Zhang, J. Wei, P. Huang, X. Zhang, B. Feng, *Journal of Material Chemistry A*, 2014, **2**, 18082.
- 56 J. Yu, W. Wang, B. Cheng, B-L. Su, *Journal of Physical Chemistry C*, 2009, **113**, 6743.
- 57 W. Li, P. Sheng, H. Feng, X. Yin, X. Zhu, X. Yang, Q. Cai, *ACS Applied Materials & Interfaces*, 2014, **6**, 12353.
- 58 P. Chang, H. Cheng, W. Li, L. Zhou, L. He, Y. Yu, F. Zhao, *Physical Chemistry Chemical Physics*, 2014, **16**, 16606.